Development of and Acceptance Test Preparations for the Thruster Component of the Ascendant Sub-kW Transcelestial Electric Propulsion System (ASTRAEUS)

IEPC-2019-283

Presented at the 36th International Electric Propulsion Conference
University of Vienna • Vienna, Austria
September 15-20, 2019

Ryan W. Conversano[1], Sean W. Reilly[2], Thomas V. Kerber[3],
John W. Brooks[4], and Dan M. Goebel[5]
Jet Propulsion Laboratory, California Institute of Technology, Pasadena, CA, 91109, USA

Abstract: A review of the development and key design aspects of the Ascendant Sub-kW Transcelestial Electric Propulsion System (ASTRAEUS) program, which aims to develop an optimized electric propulsion option enabling high-ΔV interplanetary smallsat-class spacecraft, is presented. ASTRAEUS is a Hall-thruster based low-power electric propulsion system integrating the Magnetically Shielded Miniature (MaSMi) Hall thruster with a novel ultra-compact high-performance power processing unit and a commercially available propellant flow system and gimbal. Despite the class leading performance previously demonstrated by the development model MaSMi-DM Hall thruster, a significant effort was made to advance the design to a more flight-like configuration for system integration. New hardware on the engineering model MaSMi-EM includes a fully welded & brazed heaterless LaB6 hollow cathode and a thermally isolating low-mass gimbal interface stack-up, while significant modifications to the thruster were made to improve thermal performance while reducing mass. A detailed thermal analysis performed on the MaSMi-EM, the results of which are discussed herein. Details on the vacuum facility upgrades supporting the FY20 long-duration wear test of the MaSMi-EM are also presented.

I. Introduction

IMPROVING the scientific return-on-investment for speed space missions is a key goal of the space science community and has fueled NASA's increasing interest in interplanetary SmallSat spacecraft (wet mass spanning from several 10's to several 100's of kg). SmallSats targeting both the inner solar system (Venus, Mars)[1,2] and the outer solar system (Saturn, Neptune, Uranus)[3] have been the focus of many recent mission studies. A key limitation to deep-space SmallSats is the lack of qualified long-life propulsion options. The near-Earth space environment, which is the primary target for many start-up electric propulsion (EP) companies' development efforts (SmallSat constellations, military applications, etc.)[4–9], is well-understood; further, near-Earth constellation missions generally have limited lifetime and/or performance requirements, facilitating EP subsystem development. However, using

[1] Technologist, Electric Propulsion Group, ryan.w.conversano@jpl.nasa.gov.
[2] Technologist, Electric Propulsion Group, sean.w.reilly@jpl.nasa.gov.
[3] JPL Student Intern, University of Western Michigan, thomas.v.kerber@umich.edu.
[4] JPL Student Intern, Columbia University, jwb2159@columbia.edu.
[5] JPL Fellow, Propulsion, Thermal, & Materials Engineering Section, dan.m.goebel@jpl.nasa.gov.

SmallSats to complete challenging interplanetary scientific missions is currently infeasible due to the lack of flight-proven high-throughput sub-kW EP systems in the commercial marketplace[10,11].

The Jet Propulsion Laboratory's (JPL) Ascendant Sub-kW Transcelestial Electric Propulsion System (ASTRAEUS) program aims to fill this apparent in-space propulsion technology gap and enable high-ΔV interplanetary exploration using SmallSats. ASTRAEUS is a fully integrated electric propulsion system, including a low-power Hall thruster, an ultra-compact power processing unit (PPU), a xenon flow controller (XFC, not including a tank or pressure management assembly [PMA]) using commercially available flight-demonstrated parts, and a commercial off-the-shelf (COTS) gimbal, targeting a TRL-6 classification[12] by mid-2021. This combination of new technology (PPU), maturing technology (MaSMi), and demonstrated technology (XFC, gimbal) will facilitate the system's completion and qualification by the target date through two concentrated development efforts while minimizing programmatic risk by using COTS components where available. JPL has selected commercial partner Apollo Fusion, Inc. of Mountain View CA to co-develop and fabricate ASTRAEUS hardware. Via a commercial license issued by CalTech, Apollo is also developing a simplified single-operating-point commercial system variant, AXE (Apollo Xenon Engine)[13]. All engineering model (EM) hardware for the ASTRAEUS program was provided by Apollo Fusion, including the first engineering model MaSMi-EM (Magnetically Shielded Miniature) Hall thruster shown in Fig. 1.

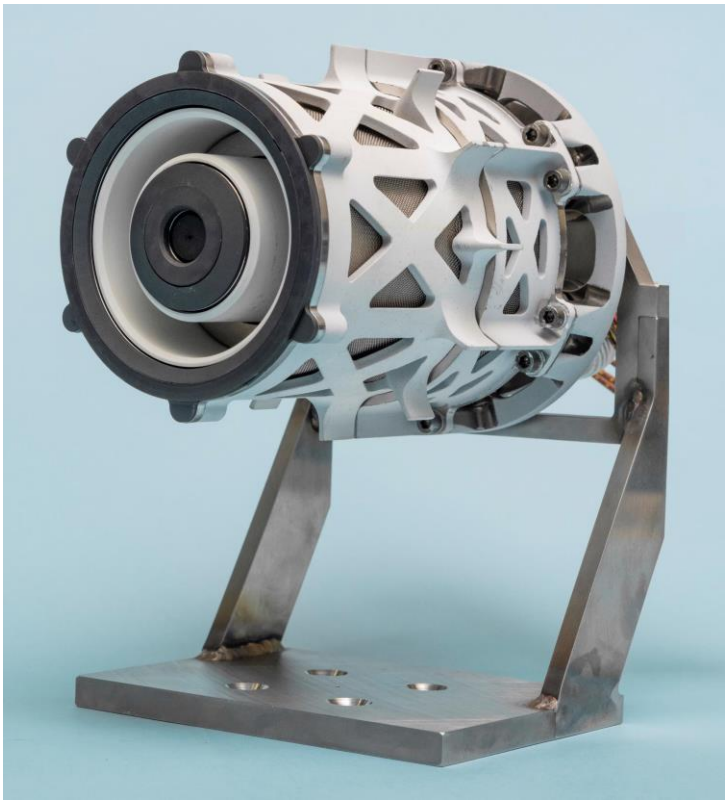

Figure 1. MaSMi-EM SN001 Hall thruster fabricated, assembled, and delivered by Apollo Fusion.

ASTRAEUS is based around the MaSMi (Magnetically Shielded Miniature) Hall thruster, which has a well-documented development history since its inception in 2011[14–23] and is the world's highest-performing sub-kW Hall thruster[24]. MaSMi is presently the world's highest-performing sub-kW Hall thruster with peak demonstrated total specific impulse and total efficiency of >1930 s and >54%, respectively[24], and an estimated propellant throughput of 100 – 500 kg Xe (depending on operating condition)[25–28]. Plots of the development model MaSMi-DM's thrust, total specific impulse, and total efficiency against discharge power at various discharge voltages is presented in Fig. 2.

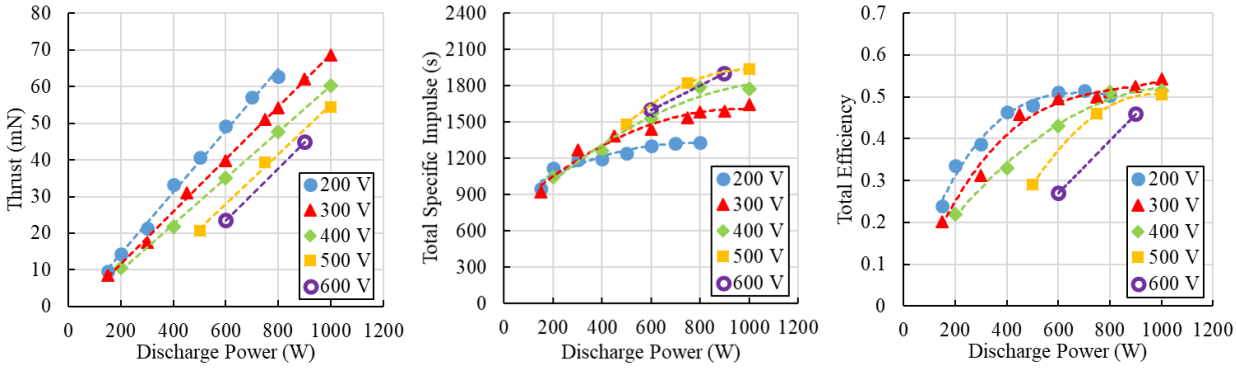

Figure 2. Thrust (left), total specific impulse (middle), and total efficiency (right) demonstrated by the MaSMi-DM Hall thruster[24].

The MaSMi and subsequent ASTRAEUS programs have followed a development approach similar to that established by NASA's 12.5 kW HERMeS (Hall Effect Rocket with Magnetic Shielding) program, now part of the Advanced Electric Propulsion System (AEPS)[29–31]. Like HERMeS, MaSMi achieves exceptionally high throughput capabilities through the application of magnetic shielding. The physics of magnetic shielding were first described by the Jet Propulsion Laboratory after Aerojet Rocketdyne's XR-5 (formerly the BPT-4000) reached a zero-erosion state 5.6 kh in to a 10.4 kh wear test[32,33]. Subsequently, magnetic shielding was shown by JPL to reduce erosion rates by three orders of magnitude in a series of simulations and experiments designed to validate the physics of magnetic shielding through modification of the H6 Hall thruster[34–38]. Magnetic shielding is now well understood with experimental and computational validation completed on numerous magnetically shielded (MS) Hall thrusters with operating powers spanning 0.15 – 20 kW[32,35–43]. A more thorough understanding of the physics governing MaSMi's operation, enabled by advancements in JPL's physics-based numerical models for the cathode and discharge chamber plasma alongside commercially available engineering tools for the magnetics design, structural analysis, and thermal analysis, facilitated its optimization to achieve class-leading performance

In this paper, we describe the design and development, of the thruster component of ASTRAEUS, i.e. the engineering model (EM) MaSMi-EM Hall thruster along with the completed acceptance testing preparations. Section II provides a review of thruster design, highlighting the key elements and developments that contribute to the thruster's class-leading performance. A brief overview of the MaSMi-EM acceptance testing preparations is presented in Section III. Concluding remarks are made in Section IV.

II. Design Overview

The MaSMi-EM is the most recent Hall thruster iteration to come from the MaSMi development program. The fundamental design features are based on the successful MaSMi-DM thruster, which demonstrated class-leading performance, throttling, and predicted lifetime[24,44]. Many of the prior design details can be found in the literature[24,44] and associated US patent[45]. As delivered from Apollo Fusion, the MaSMi-EM (including all gimbal mounting hardware & fasteners, harness & connector, but excluding the thrust stand interface mount shown in Fig. 1) had a mass of 3.38 kg which meets the thruster mass requirement[28].

A. Magnetic Circuit Design

Like all generations of the MaSMi thruster before it, the MaSMi-EM uses an primarily axisymmetric thruster geometry with concentric electromagnetic coils[21,23,46]. This is beneficial both from a magnetics performance standpoint as well from a plasma modeling and correlation standpoint[47–49]. The magnetic circuit provides a fully shielding magnetic field topology across the full range of necessary field strengths. Additionally, the magnetic circuit provides field strength margins against pole saturation over the thruster's entire designed service life. For the first time in a MaSMi thruster, the magnetic circuit was optimized to provide a symmetric field topology (relative to the discharge channel centerline) across the required range of field strengths (including margin) with the electromagnetic coils operated in series. Doing so eliminated a magnet coil power converter from the ASTRAEUS PPU, thereby reducing PPU (and therefore system) mass, volume, and complexity.

One of the most obvious features of the MaSMi-EM thruster are the many cut-outs found throughout the magnetic circuit, as seen in Fig. 3. During initial stages of the thruster design process, it was discovered that several regions of

the MaSMi-EM magnetic circuit (e.g. the outer guide) were at no risk of magnetically saturating over the necessary range of field strengths. Material could therefore be removed from these regions without modifying the external magnetic field topology generated by the thruster. This would have the coupled benefits of reduced thruster mass and improved thermal radiation from the outer coil (discussed further in Section II.E) The removal of this material, however, had to be balanced with the structural requirements of the device which were derived from the dynamic and thermal environmental requirements[28]. An iterative optimization process followed, culminating in the finalized MaSMi-EM design. Combining the effects of the magnetic circuit optimization and electromagnet coil balancing for in-series operation, the thruster mass was reduced by nearly 0.5 kg.

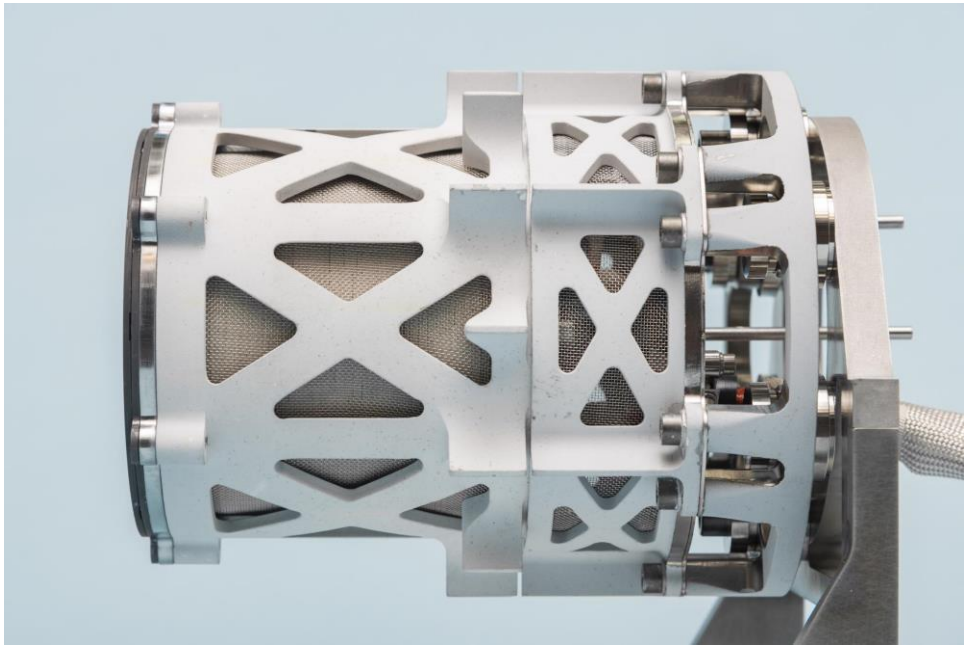

Figure 3. Side view of the MaSMi-EM SN001 Hall thruster.

B. Pole Cover (i.e. Erosion Mitigation) Design

As with all magnetically shielded Hall thrusters, the discharge plasma of the MaSMi-EM is shifted downstream compared to unshielded Hall thrusters, extending beyond the thruster exit plane. While this is a natural byproduct of the MS field topology that eliminates discharge channel erosion, it has been demonstrated to increase magnetic pole erosion[31,40,48,50–52]. The engineering solution to mitigate pole erosion was the introduction of sacrificial graphite pole covers mounted on the downstream faces of the thruster's magnetic poles. Graphite was selected due to its significantly lower sputter yield under Xe ion incidence (by a factor of 5-10x) than typical magnetic pole and fastener materials. Graphite pole covers have been successfully integrated on high-power (HERMeS/AEPS)[29–31], mid-power (H6MS, H9MS)[48,52,53], and low-power (MaSMi) Hall thrusters[24,44] with no observable detriments to thruster performance.

An image of the MaSMi-EM pole covers installed on the thruster is shown in Fig. 4. The MaSMi-EM uses pole covers with a chamfered edge facing the discharge channel to provide some shadow-shielding to the pole cover fasteners from the primary plasma beam. These fasteners are further protected by a downstream graphite cover of the same thickness as the thinnest part of the primary pole cover. The pole cover thickness was sized to protect the magnetic poles from exposure to Xe ion bombardment erosion over a minimum propellant throughput of 100 kg Xe under the highest erosion operating conditions, which occur at the lowest operating voltage (200 V) and powers ($\leq$200 W) within the ASTRAEUS throttling range[25]. An advantageous byproduct of this design is that, because the observed erosion rates at higher powers (approx. >300 W at 200 – 500 V) is up to 5x lower than at low voltage & power, a comparable increase in the thruster's projected propellant throughput capability can be expected[25].

Figure 4. The graphite pole covers on the MaSMi-EM SN001 Hall thruster.

C. Cathode Design

The MaSMi-EM accepts the EM variant of the heaterless lanthanum hexaboride (LaB_6) MaSMi's LUC (Low-current Ultra-compact hollow Cathode)[45] located along the thruster's centerline axis. Internally mounted cathodes provide a Hall thruster with numerous benefits compared to their external cathode counterparts. Thruster performance and efficiency can increase by as much as 5% when using an internally-mounted cathode compared to an external cathode[54–56]. Reduced discharge oscillations, improved cathode-thruster coupling (i.e. lower cathode-ground voltage), improved plume symmetry, and decreased beam divergence (i.e. improved thruster performance) have also been observed[54–56]. Perhaps most importantly, internal cathode thruster configurations have been demonstrated to have minimal sensitivity to vacuum facility background pressure effects, thereby significantly improving the correlation between ground tests and flight performance[54–58].

Previous versions of MaSMi's LUC have been successfully demonstrated and tested using both barium oxide impregnated tungsten (BaO-W) and LaB_6 thermionic emitters and in both a heater and heaterless configuration[24,44]. The useful life of the LaB_6 emitter found in the EM MaSMi's LUC was predicted using an evaporation model of the LaB_6 emitter (which assumed no redeposition of emitter material which can extend emitter life)[24]. The model suggested that the cathode would conservatively provide a minimum 3x life margin against the thruster propellant throughput requirements[24] at the highest current condition in the ASTRAEUS throttle range, which is assumed to correspond to the highest emitter depletion rate and therefore the shortest emitter lifetime. Validation of the cathode throughput capability is currently underway in the form of a combined ignition cycle and long-duration wear test[28].

The ASTRAEUS EM cathode is a fully welded and brazed design. It incorporates a graphite keeper to mitigate Xe ion bombardment erosion from the cathode plume and primary plasma beam. The keeper thickness is significantly greater than that of the graphite pole covers to provide margin against wear-out and orifice diameter expansion effects should the erosion rates on the keeper face be of the same order of magnitude as those on the poles. Based on prior testing of other MS Hall thrusters, which showed significantly lower keeper face erosion than pole erosion[59,60], the MaSMi-EM cathode keeper design should be conservative.

D. Anode Design

The MaSMi-EM uses a similar anode (including the manifold and gas distributor) to that first demonstrated on the MaSMi-DM. The anode, conceived during prior MASMi developments[21,22] and described in U.S. Patent Application No. 16/205,048[37], generates a primarily radial propellant flow pattern which significantly improves propellant utilization and azimuthal flow uniformity. The DM unit demonstrated sub-3.2% peak-to-peak (±1.6%) azimuthal flow non-uniformity across two anodes and across a range of relevant flow rates[24,44]. A selection of these data is presented in Fig. 5. This is significantly lower than both NASA's accepted standard of ±5% non-uniformity and published results for several recent thrusters across multiple power regimes[61,62]. Flow uniformity testing of the MaSMi-EM is planned during acceptance testing of the thruster; based on the inspection reports from the MaSMi-EM anode components, the uniformity results are expected to be in family with the DM anode.

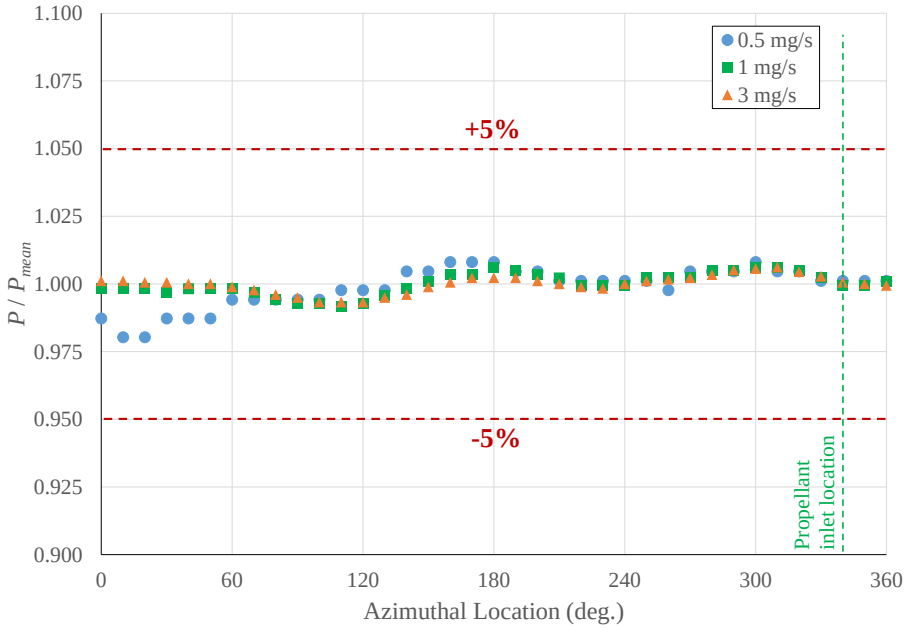

Figure 5. Azimuthal propellant flow uniformity profiles for the MaSMi-DM anode manifold SN002[24].

E. Thermal Design

Thermal Challenges: Heat management in magnetically shielded Hall thrusters has proven to be a non-trivial aspect of the overall thruster design process, highlighted by the recent HERMeS/AEPS development program[63,64]. Despite the thruster's high demonstrated total efficiency, which corresponds to lower heat dissipation requirements, the thermal design of the MaSMi-EM posed many challenges. These include:

High-voltage operation: While this provides the benefit of MaSMi-EM's nearly 2000 s of total specific impulse, it also correlates to higher operating temperatures. Increasing thruster power clearly increases the heat load on a Hall thruster. However, testing of the MaSMi-DM at a constant discharge power 1000 W and 300 V, 400 V, and 500 V revealed that the higher voltage conditions yielded higher thruster temperatures at a given magnet current setting. This is attributed to the higher electron energies generated as the discharge voltage is increased, which subsequently increases sheath potentials on the thruster surfaces and the therefore the energy of collected Xe atoms. This observation suggests that, at least in the MaSMi-DM, higher sheath potentials (i.e. the discharge voltage) has a larger contribution to thruster temperature than plasma density (i.e. discharge current).

Low surface-to-volume ratio: As is common for low-power Hall thrusters, the MaSMi-EM suffers from a low radiating surface area relative to its total volume. This is true for both the discharge channel and the entire thruster. Ultimately, this translates to the thruster having difficulty rejecting sufficient heat via surface radiation to prevent temperatures from rising beyond internal component limitations.

Poor thermal conductivity materials: The majority of the MaSMi-EM is comprised of high magnetic permeability material, as required by the magnetic circuit design. Unfortunately, the thermal conductivity of most high-permeability materials is poor at room temperature (<100 W/m-K) and worse at typical Hall thruster operating temperatures (<50 W/m-K). This prevents heat generated inside the thruster (especially, the magnet coil power) from being effectively conducted to the primary radiating surfaces along the thruster's exterior.

Ultra-compact LaB_6 hollow cathode: LaB6 requires higher temperatures to generate a given current density than most alternative cathode emitter materials[65]. This feature, coupled with the compact size of the cathode (see the low surface-to-volume ratio argument above), yields high cathode temperatures in and around the emitter. Although insufficient thermal isolation leads to both higher coupling voltages and therefore reduced thruster performance, isolating the cathode power to the emitter region yields higher localized temperatures which cause increased local conduction and radiation to the thruster's internals.

Power conduction requirements: Based on the tight thermal budgets of the smallsats likely to fly ASTRAEUS, the ASTRAEUS program self-imposed a requirement of $\leq$5 W of steady-state thermal power conduction from the thruster to the spacecraft across all operating conditions. This requirement forces difficult design choices between

varying the amount of thermal isolation during thruster operation and the associated variation in thruster temperature during periods of non-operation.

No survival heaters: Survival heaters are a common method to keep thruster temperatures at or above a specific limit, which can aid in qualification of the device. The MaSMi-EM's steady-state operating temperatures at or near 1000 W exceeds the temperature limits of most survival heaters and their adhesives. The limited surface area available for heater placement limits the use of bolt-on high-power resistor heaters. Additionally, Kapton film heaters typically have a temperature limit around 150°C due to their Teflon inserts, well below the operational temperature of the thruster. While high temperature Kapton film heaters exist, used as replacements for the Teflon inserts and coupled with more robust metal traces, their temperature limits still only extend to about 250°C which is still not high enough to safely be used on the thruster. Furthermore, the concept of using the magnet coils to heat the thruster was rejected as it would require the PPU to be powered whenever the thruster needed to be warmed (a major problem during spacecraft safe-mode operations, for example). Therefore, the decision was made to design and qualify the thruster to survive in its required environments[28] without the use of survival heaters.

Thermal Challenge Mitigation: In order to overcome the numerous difficulties associated with a 500 V – 1000 W capable Hall thruster with a compact form factor, a major focus was placed on thermal management through the thruster design process. The resulting MaSMi-EM incorporates several key features that enable adherence to the ASTRAEUS thruster requirements[28]. These include:

Radiation fins: The MaSMi-EM utilized radiation fins to improve radiative heat rejection. One set of fins are located on the upstream lateral surface of the magnetic circuit. The design and placement of the magnetic circuit fins was the result of an iterative design optimization process performed using a correlated thermal model of the thruster. A selection of fin designs (axially short, axially long, radially short, radially tall, narrow base, wide base, triangular, etc.) were considered. The selected design was a wide based, tapered fin (closely matching a nominal radiative fin design[66]) with an axial length slightly longer than the backpole thickness and a maximum outer diameter equal to that of the gimbal interface. The fins were located immediately radially outward from the thruster backpole, which facilitates heat transfer from the thruster's internals to these radiating surfaces without the need for conduction along the thruster's axial outer magnetic guide. These fins can be seen in the detail image of the MaSMi-EM shown in Fig. 6.

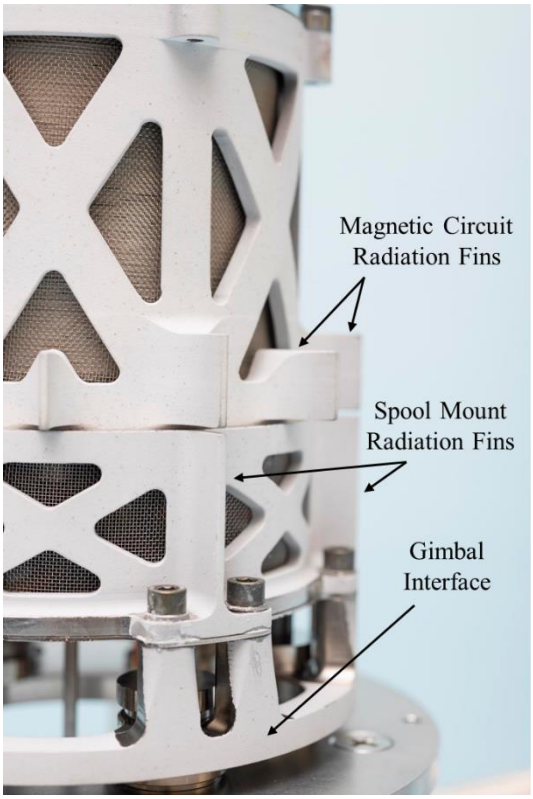

Figure 6. Detail image of the MaSMi-EM SN001 showing the radiation fins integrated into the magnetic circuit and spool mount.

A second set of radiation fins are integrated into the spool mount, which provides an interface between the thruster head and the gimbal interface. These were added as a means to improve the thermal isolation of the thruster head by rejecting a portion of the heat conducted upstream towards the gimbal interface. The spool mount fin design was based on that of the magnetic circuit fins; no iterative design process was used to further optimize them.

Exterior surface coating: Nearly all non-mesh outward-facing surfaces of the thruster are coated with a high-emissivity low-absorptivity coating resistant to property changes with carbon backsputter. This can be seen in Figs. 1, 3, and 6. The coating significantly increases the surface emissivity when compared to bare machine-finished metal, improving radiative heat rejection by >>10x. Despite this high emissivity, the white coating also maintains a low overall absorptivity which reduces absorbed power from environmental heat sources. The coating's resistance to changes to emissivity and absorptivity during a long-duration ground testing in which carbon backsputter is expected to be present improves the relevance of the test results to a spaceflight environment.

Integrated cut-outs: As discussed in Section II.A, unneeded material was removed from the magnetic circuit to reduce thruster mass. The fortunate byproduct of this design is the creation of "windows" for the outer electromagnetic coil to view the space environment. This yields greater heat rejection efficiency by providing a cold radiative heat sink for the coil compared to a solid outer magnetic core where the coil's thermally radiated power is collected by the

magnetic circuit, conducted (relatively inefficiency) to a radiating surface, and then rejected. A similar mass reduction philosophy, along with the associated thermal benefits, was applied to the spool mount. Adding cut-outs reduces the total amount of material between the thruster head and gimbal interface, thereby providing a choke to upstream thermal conduction. Lastly, the gimbal interface was designed to contain as little material as possible to minimize mass and further reduce thermal conduction to the gimbal.

Thermal Modeling Results & Validation: As mentioned previously, the MaSMi-EM thermal design is an evolutionary step forward from the MaSMi-DM. Many of the design features mentioned in the previous section were the result of design trades intended to improve thermal margins on the thruster during hot operation.

In order to explore this trade space, a previously correlated MaSMi-DM model was used as a starting point. During prior testing[24], the MaSMi-DM was instrumented with 3 type K thermocouples (±2.2°C or 0.75% uncertainty): one on the backpole (upstream side of the core, facing the gimbal), one on the outer front pole, and one on the inner coil. The MaSMi-DM was run to thermal steady state and allowed to "soak" at this state in order to characterize the performance. Thermal steady state was assumed to have been reached when a thermocouple placed on the backpole showed a temperature rate of change of less than 2°C/hr. This temperature location is one of the last locations to reach steady state and as a result, envelopes the majority of the thruster in terms of temperature gradients.

Correlating a detailed thermal model of the MaSMi-DM involved many unique challenges; however, the DM model was successfully correlated by making slight adjustments to 3 parameters:

- Plasma thermal loading of the thruster
- Optical properties of the thruster
- Contact conductances between the thruster components

The largest source of uncertainty in the correlation process is the adjustment of the thermal plasma loading. Hall thruster thermal modeling reports thermal plasma loads to be anywhere from 8% to as high as 20%[63,67]. For JPL development efforts, the thermal plasma loading was estimated using Hall2De[67] which itself is temperature dependent for its predictions. While this may appear to be a relatively small variation in thermal loading (8 – 20% of 1000 W yields 80 – 200 W), tens of watts have a significant impact on the temperature response of the MaSMi thruster due to its small size.

Optical properties are taken as temperature dependent values when available, but not all materials used in the thermal model have referenced temperature dependent properties and therefore introduce some additional uncertainty. The optical property was initialized at whatever most appropriate literature value could be obtained and was adjusted (within reasonable bounds) to achieve correlation.

Contact conductance is the final adjustment parameter in the model and is the most deterministic of the three since most of the interfaces between thruster components are bolted joint interfaces, for which there are many references to draw from[68]. There may be some variation in these values as the high thruster temperatures can theoretically affect the contact surface area between components. The MaSMi-DM and -EM are outfitted with Belleville washers where appropriate to maintain pre-load. While the thermal model varied optical and contact properties, generally the optical properties and contact conductances do not vary greatly from literature values (typically <20%)[69] and the majority of the uncertainty derives from the determination of the thermal plasma loading.

Rolling up the thermocouple measurement uncertainty and the model parameter uncertainty, the MaSMi-DM model was correlated to within ±10°C which is considered reasonable given the sources of uncertainty present in the model. The thermal plasma loading was found to be simulated as 19% of the total discharge power of the thruster, which was within previous reported literature values. The optical and contact conductance properties were also all within reasonable variation to reported values[69].

With a correlated DM model, several design trades were completed to improve the thermal margin of the MaSMi-EM thruster. Fins were the primary modification to the thruster design that the thermal model examined. The conduction path from the highest temperature components (cathode, discharge channel, inner electromagnetic coil) to the radiating surfaces consists of low-conductivity materials (see *Thermal Challenges* above) and must cross interface resistances to be rejected to the environment. Fins integrated into the outer magnetic guide were the most straightforward method to improve heat rejection of the thruster core. However, this design decision was complicated by the fact that fins add mass and that they must not interfere with the integrated cutouts, which left minimal area on which to attach thermally efficient fins.

The design process began with the baseline MaSMi-EM, the magnetic core of which is shown in Fig. 7, which did not employ radiation fins. While several finned magnetic core designs were considered, two will be presented in this paper. The first design, which was ultimately not selected, aimed to maximize the core exterior surface area by making long, thin fins that ran the length of the core (see Fig 8). In order to maintain the thruster footprint, the fins did not extend radially beyond the outer front pole fastener bosses and therefore had a limited overall height. The fins were also required to be monolithic with the core structure to prevent the use of bulky bolted joint interfaces, necessitating their construction from low thermal conductivity material. Thermal analysis revealed that this fin design was not effective due to their low thermal conductivity, which required heat to be conducted axially along the core and then into the fin to be rejected. The fin efficiency was also low due to the narrow interface with the magnetic core, which caused much of the fin height to be unutilized since heat was not effectively conducted along the full height of the fin.

The lateral surface of the backpole (essentially, the upstream ~1 cm of the outer guide) represents the highest space-facing temperature of the core's exterior. The fin design was therefore targeted to that region to maximize thermal efficiency; functionally, this yields a higher temperature gradient across the fin than is possible with fins located further downstream along the core. The fins were reworked to be axially short, wide-based, and tapered to locate a greater fraction of fin material near the base while exposing more surface area to the environment. This significantly improved fin efficiency over the long axial fins and was ultimately incorporated into the MaSMi-EM design. A comparison between MaSMi-DM test data, the MaSMi-DM thermal model, and the MaSMi-EM thermal model is presented in Table 1.

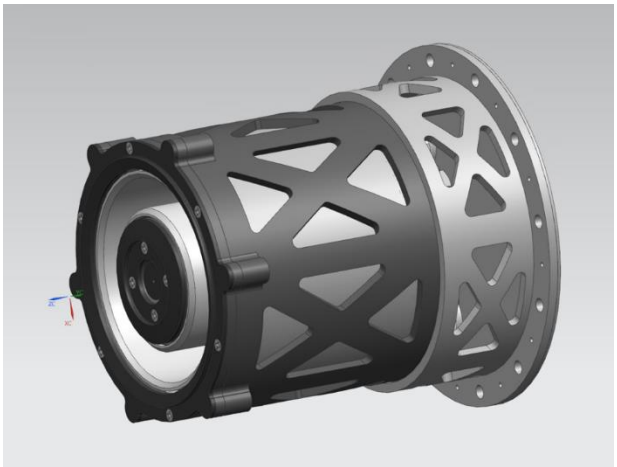

Figure 7. MaSMi-EM original baseline magnetic core design (no fins).

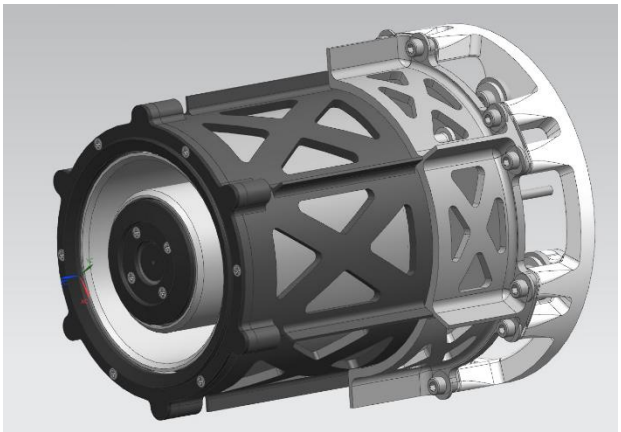

Figure 8. MaSMi-EM magnetic core with early fin design (axially long, thin fins).

Table 1: Experimental and Simulated Temperatures for the MaSMi-DM and MaSMi-EM Operating at 500 V – 1000 W

Location	MaSMi-DM (Measured)	MaSMi-DM (Correlated Prediction)	MaSMi-EM w/ Optimized Fins (Prediction)
Backpole	338°C	346°C	311°C
Outer Front Pole	288°C	281°C	217°C
Inner Coil	437°C	429°C	380°C

Thermal predictions of the MaSMi-EM with optimized radiation fins operating at 500 V – 1000 W in a ground-test facility environment can be seen in Fig. 9. The thermal optimization of the MaSMi-EM resulted in significant (35 – 64°C) reductions in predicted temperatures throughout the thruster during operation at compared to the MaSMi-DM operating at the same condition. A noteworthy risk of adding passive radiation fins is that they are always functioning, even when the thruster is not operating. As mentioned above, no survival heaters are used on the MaSMi-EM thruster since they would not survive the thruster's normal operating temperatures. It was therefore necessary to simulate the thruster's temperature response when in deep space with a fixed -50°C minimum gimbal

temperature (based on reported limits of the design gimbal hardware[28]). The result, shown in Fig. 10, shows the thruster modeled in a non-operational state in full view of deep space (i.e. with no heat sources and a background temperature of 2.7 K) with a fixed upstream boundary at -50°C. The thruster is predicted to maintain temperatures above -120°C (corresponding to a minimum of -106°C at any of the three locations listed in Table 1) without the use of survival heaters, requiring qualification of the thruster hardware beyond this point[28].

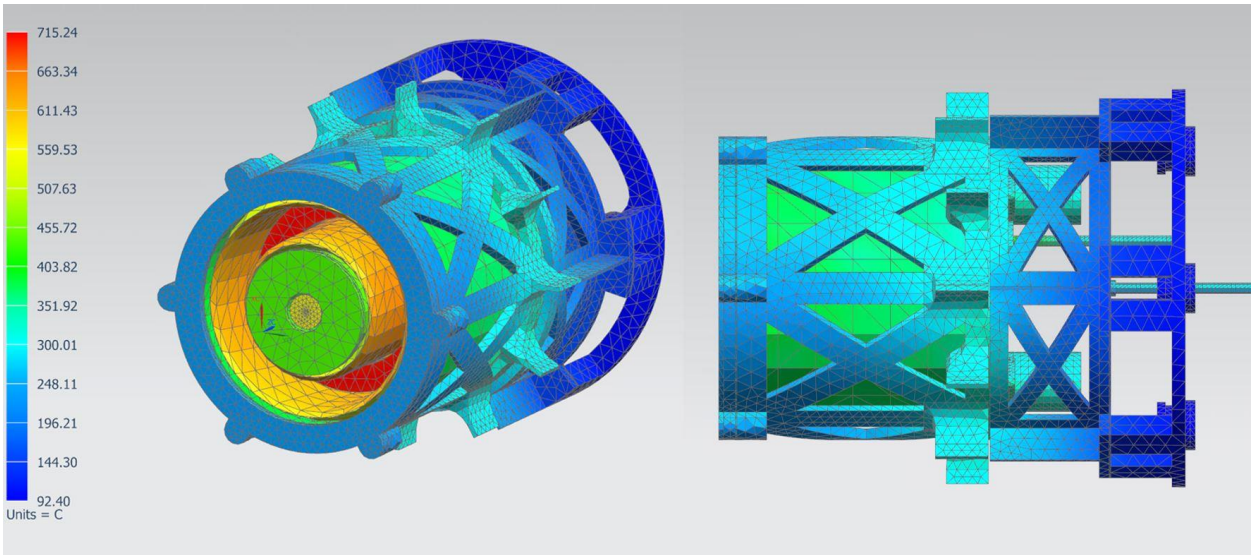

Figure 9. MaSMi-EM temperature predictions at 500 V – 1000 W in a ground test facility environment (note that the significantly higher ground facility background temperature yields higher predicted gimbal interface temperatures compared to the deep-space predictions[28]).

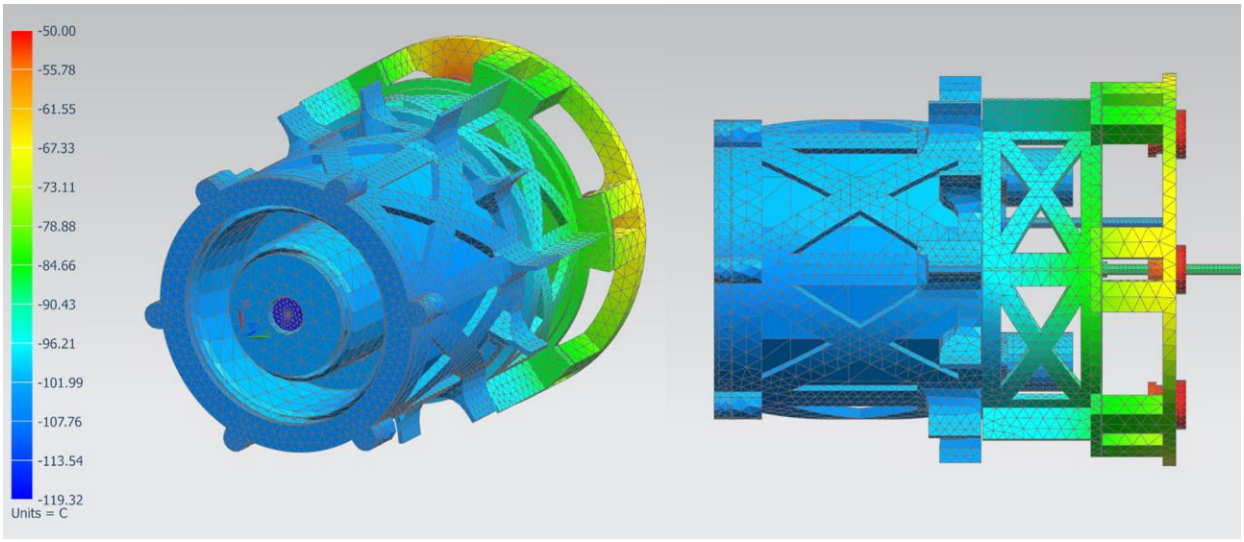

Figure 10. MaSMi-EM temperature predictions while not operating and in a deep-space environment with a -50°C gimbal boundary temperature.

III. Test Facility Preparations

A. Vacuum Facility

Experiments were conducted at JPL's recently upgraded High-Bay vacuum facility. The High-Bay facility is a 2.6 m diameter by 5.2 m long cylindrical vacuum chamber. All internal surfaces of the chamber with line-of-sight to the thruster's discharge channel are covered with either graphite panels or carbon felt. The chamber pressure is monitored by two ionization gauges calibrated for xenon. The first gauge uses an S-shaped snorkel inlet and is positioned in the thruster exit plane approximately 60 cm radially from the thruster axis (the midpoint between the thruster and chamber wall); this is used as the primary indication of chamber pressure. The second gauge is mounted along the chamber wall at the downstream end of the vacuum chamber. Both ion gauges had a plasma screen (i.e. metallic mesh) at their respective inlets. Commercially available power supplies and propellant flow controllers are used for all experiments. Research-grade (99.9995%) Xe is supplied to the thruster via electropolished stainless steel propellant lines.

Until a recently completed pumping speed upgrade, the High Bay vacuum facility used three cryogenic pumps to generate ~35-40 kL/s on Xe. This facility configuration can be seen in the left image of Fig. 11. The tank pressures was 1.6×10^{-5} Torr during thruster operation with a total Xe flow rate of 4.7 mg/s. In preparations for an upcoming long-duration wear test of the MaSMi-EM[28], the High Bay facility underwent a pumping speed upgrade. The pre-existing pump on the chamber door, capable of handling a 40 W load at 40 K, was removed and replaced with a high-capacity "super-thumper" cryogenic pump capable of processing 135 W at 40 K. Two additional "super-thumper" (135 W @ 40 K) high-capacity pumps were installed to the left and right of the thrust stand, each shadow-shielded with a thruster-facing graphite panel backed with 12-layer multi-layer insulation (MLI) facing the pumps' cryo-sails (see Fig. 12). One additional "thumper" (90 W @ 40 K) high-capacity pump was added downstream of left "super-thumper" pump; this new pump was also shadow-shielded from the thrsuter via a 3-layer stack of alternating carbon felt and 12-layer MLI (see Fig. 13). A 30 cm inlet diameter high-capacity turbomolecular pump was installed on a ceiling port of the chamber to aid in the removal of light gases not efficiency pumped by cryogenic sails. Note that the four new cryopumps were repurposed after the 2017-2018 pumping speed upgrade of JPL's Owens vacuum facility. The High Bay's pre-existing DynaVac cryo-tub (coupled to an APD DE208L cold-head) and CVI Torr Master 1200i, both of which use a cryogenically cooled charcoal array with integrated LN_2 backing shroud, were left in place. The updated facility configuration is shown in the right image of Fig. 11.

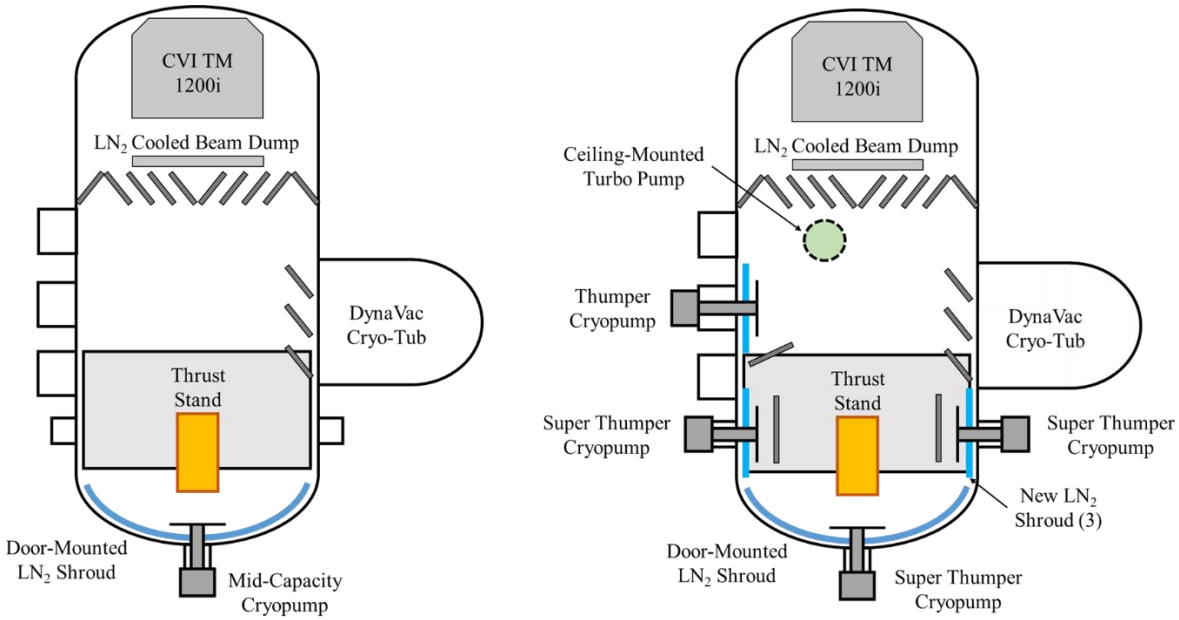

Figure 11. JPL's High Bay vacuum facility in its original ~35-40 kL/s Xe configuration (left) and upgraded ~70 kL/s Xe configuration (right).

The cryo-sails mounted to the four new high-capacity pumps are semi-polished high thermal conductivity aluminum discs with an outer diameter of 1 m. Each of the three new high-capacity pumps' cryo-sails mounted along the chamber's lateral ports are backed with new liquid nitrogen (LN_2) shrouds; the three cryo-sails associated with these new shrouds have a single flat edge matching the width of the shroud. All of the cryogenic pumping surfaces, including those of the pre-existing pumps, were instrumented with cryogenic diodes to monitor temperatures.

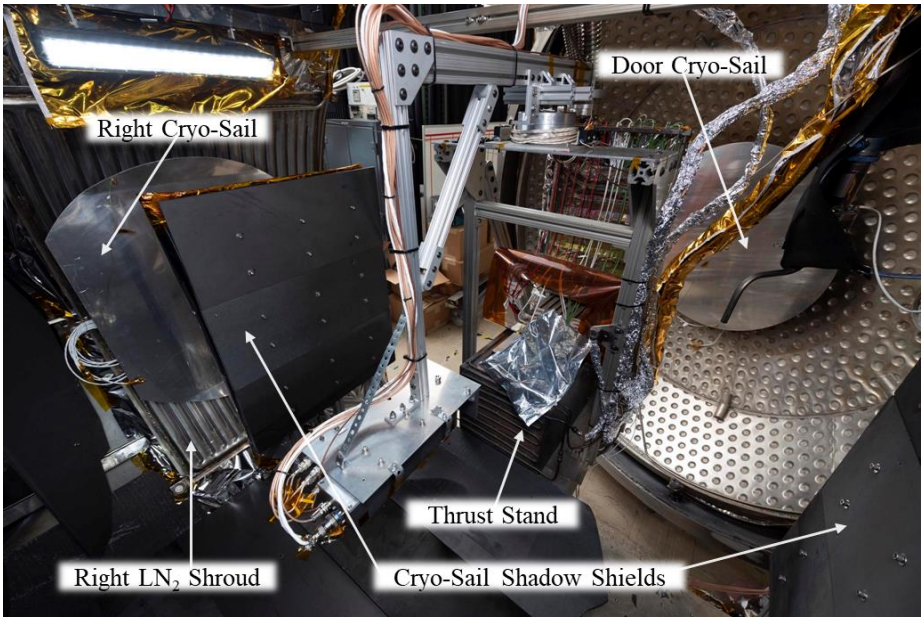

Figure 12. An upstream-facing view of the internals the JPL High Bay vacuum facility, highlighting the new cryogenic pumping surfaces and associated shadow shields.

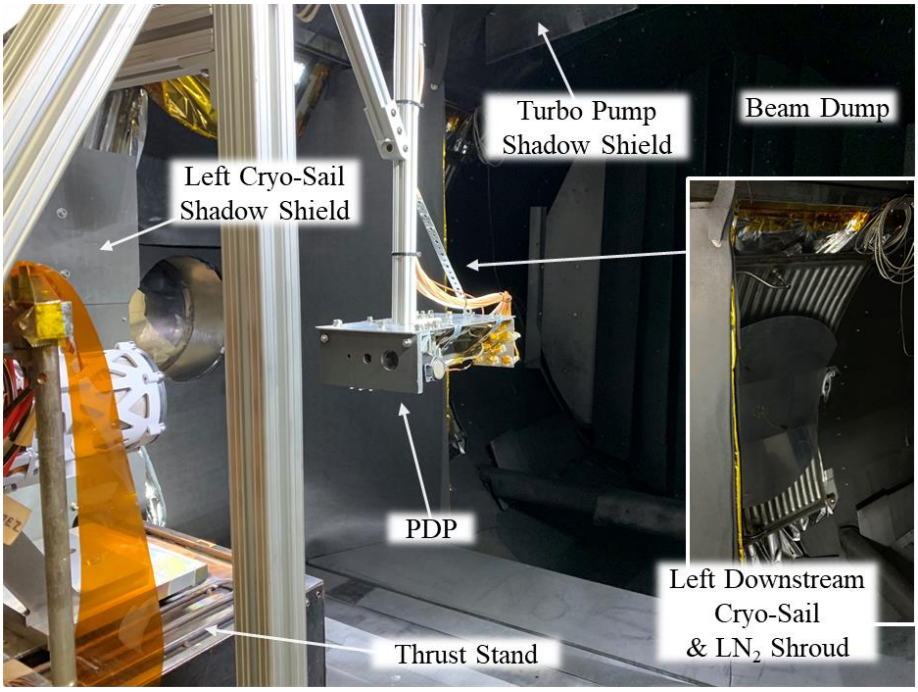

Figure 13. A downstream-facing view of the internals the JPL High Bay vacuum facility, highlighting the new cryogenic pumping surfaces and associated shadow shields.

The facility pumping speed was characterized using the following method. First, a rough vacuum was established, followed by turning on the turbo pump and flooding of the LN_2 shrouds. A vacuum of $<3x10^{-6}$ Torr was established before characterization of the turbo commenced. Due to the low known pumping speed of the turbo pump (rated at ~4 kL/s on N_2) compared to cryogenic pumps, an applied Xe flow rate was set at 0.24 mg/s from a propellant tube oriented such that the outlet was close to the location of a thruster mounted on the thrust stand. The flow was then stopped and each of the cryogenic pumps was turned on one at a time. After each pump had reached ~20 K at the center and edge as indicated by the sail's cryo-diodes, a Xe cold flow of 4.7 mg/s was established. The pumping speed was then calculated for the set of operational pumps, enabling the determination of the pumping speed for each individual pump. Results from this pumping speed measurement are shown in Table 2. The measured pressure with all pumps operating and a 4.7 mg/s Xe cold flow was $8.7x10^{-6}$ Torr, corresponding to an overall pumping improvement of ~2x over the prior facility configuration. Based on these results, which are considerably lower than the expected new pumping speed (~150 – 200 kL/s), it appeared that the efforts to shield the thruster (i.e. heat source from both radiative heat and plasma loading) from the cryo-sails yielded significantly reduced conductances to the pumping surfaces, translating to low calculated pumping speeds. Additionally, the two pre-existing pumps (CVI and DynaVac) performed at less than 20% their previously demonstrated capability despite achieving sub-25 K temperatures at the measurement locations. The facility configuration will therefore be investigated and modified to improve the conductance to each of the cryo-sails and determine the cause for the low pumping speeds of the pre-existing pumps prior to thruster hot-fire testing.

Table 2. JPL High Bay Vacuum Facility Cold Flow Pumping Speed Characterization

Pump Location / Designation	Pump Capacity *W @ 40 K*	Xe Flow Rate *mg/s*	Pumping Speed *kL/s on Xe*
Turbo pump	-	0.24	1.8
Chamber door	135	4.7	26.2
Right of thruster	135	4.7	14.3
Left of thruster	135	4.7	14.4
Left downstream	90	4.7	8.1
DynaVac	35	4.7	2.5*
Beam dump	35	4.7	2.7*
TOTAL	-	-	**70.0**

* These pumps demonstrated considerably lower performance than previously recorded; warranting future investigation.

B. Thruster Diagnostics

A water-cooled inclination-controlled inverted-pendulum thrust stand was used to measure the thrust of the MaSMi-DM. The thrust stand uses an optical-based displacement sensor which is correlated to thrust by lowering and raising a series of precision masses. The thrust stand consistently demonstrates a resolution of 0.1 mN with an estimated uncertainty of ±1.0%. Combined with the other thruster system uncertainties (power supplies, flow controllers, etc.), the estimated uncertainty in specific impulse and efficiency are ±1.1% and ±2.1%, respectively. An image of the thrust stand with the MaSMi-EM in place is shown in Fig. 14.

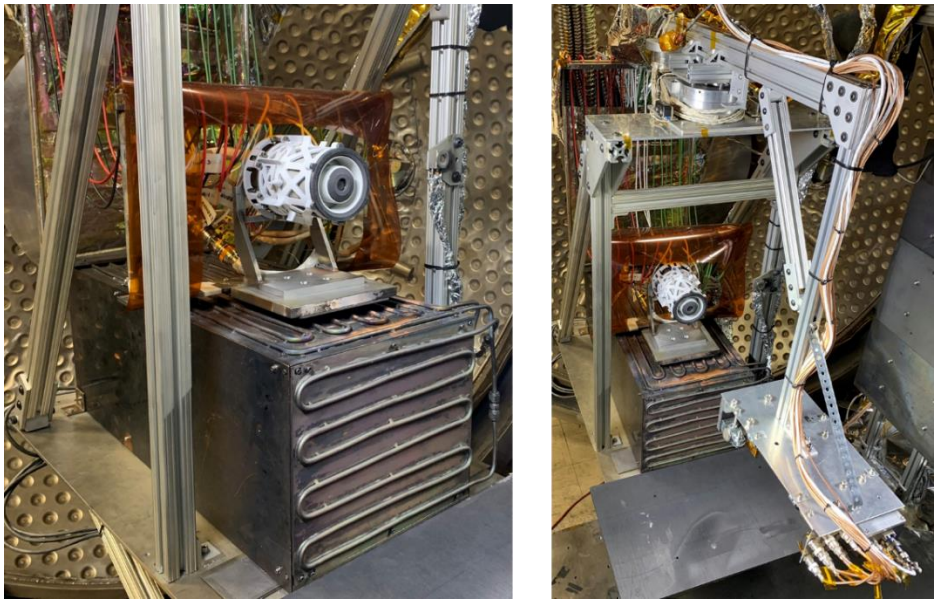

Figure 14. High Bay facility thrust stand with MaSMi-EM in place. The left image shows a detail view of the thrust stand while the right image includes the PDP rotary stage mounted above the thrust stand.

C. Plasma Diagnostics

A plasma diagnostics package (PDP) consisting of an **E**x**B** filter, a retarding potential analyzer, a shielded Faraday probe, a shielded planar Langmuir probe, and three emissive probes was added to the High Bay vacuum facility. The PDP is mounted at the end of a boom extending from a rotary motion stage with the axis of rotation located in-plane with both the thruster exit and the thruster centerline axis. The PDP's upstream face is located 5 discharge channel lengths downstream of the thruster when oriented immediately downstream of the thruster. An image of the PDP installed in the High Bay vacuum facility is shown in Fig. 15. The rotary stage to which the PDP is mounted can be seen in Fig. 14.

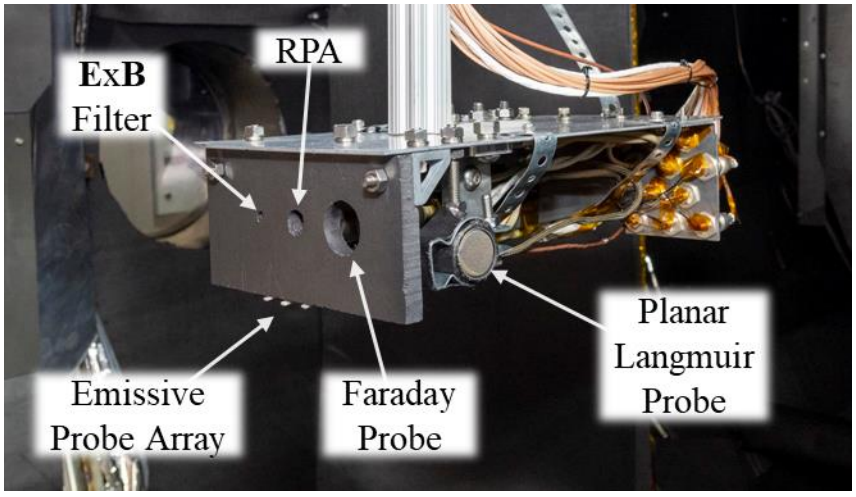

Figure 15. Detail view of the High Bay facility plasma diagnostics package.

IV. Conclusion

An overview of the development and design of the thruster component of the Ascendant Sub-kW Transcelestial Electric Propulsion System (the engineering model MaSMi-EM Hall thruster) was presented. Details of the MaSMi-EM's magnetic circuit, pole cover, anode manifold, and cathode were covered. The MaSMi-EM thermal design was

evaluated using a previously correlated thermal model developed for the MaSMi-DM and adapted to the MaSMi-EM geometry. The MaSMi-EM was shown by analysis to significantly improve thermal margin during thruster operation compared to its predecessor while maintaining sufficiently high temperatures when cold to eliminate the need for survival heaters. A recent vacuum facility pumping speed upgrade supporting an FY20 long-duration wear test of the MaSMi-EM yielded a pump rate of 70 kL/s on Xe, improving the facility's pumping speed by a factor of ~2x compared to its original configuration. Future improvements will be made to further improve this pumping speed prior to the start of the long-duration wear test. A brief review of the plasma diagnostics found in the High Bay vacuum facility was also presented.

Acknowledgments

The authors would like to recognize the efforts of Apollo Fusion to deliver ASTRAEUS EM hardware to the stringent JPL requirements throughout the 2019 fiscal year. We would also like to thank Ray Swindlehurst (JPL) and Nowell Niblett (JPL) for their assistance in setup and maintenance of the vacuum facilities utilized in this effort. This research was carried out at the Jet Propulsion Laboratory, California Institute of Technology, under a contract with the National Aeronautics and Space Administration and funded through the internal Research and Technology Development program.

References

[1] Sutin, B. M., Cutts, J., Didion, A. M., Drilleau, M., Helbert, J., Karp, A., Kenda, B., Komjathy, A., Krishnamoorthy, S., Lantoine, G., Lognonné, P., Makela, J., Nakazono, B., Rud, M., and Wallace, M., "VAMOS : a SmallSat mission concept seismic activity from orbit," *SPIE, Journal of International Society for Optics and Photonics*, Jul. 2018, DOI: 10.1117/12.2309439.

[2] Woolley, R., and Olikara, Z., "Optimized Low-Thrust Missions from GTO to Mars," *2019 IEEE Aerospace Conference*, Big Sky, MT: 2019.

[3] Conversano, R. W., Rabinovitch, J., Strange, N. J., Arora, N., Jens, E., and Karp, A. C., "SmallSat Missions Enabled by Paired Low-Thrust Hybrid Rocket and Low-Power Long-Life Hall Thruster," *2019 IEEE Aerospace Conference*, Big Sky, MT: 2019.

[4] Apollo Fusion Inc., "Apollo Constellation Engine (ACE)" Available: http://apollofusion.com/index.html.

[5] ExoTerra Resource, "Halo Micro Hall Effect Thruster" Available: https://exoterracorp.com/?p=114.

[6] Lev, D., and Appel, L., "Heaterless Hollow Cathode Technology - A Critical Review," *Space Propulsion 2016*, SP2016-3125366, Rome, Italy: 2016.

[7] Kim, V., "Stationary Plasma Thrusters in Russia : Problems and Perspectives," *Journal Trudy MAI (Moscow Aviation Institute)*, vol. 60, 2014.

[8] Szabo, J., Pote, B., Tedrake, R., Paintal, S., Byrne, L., Hruby, V., Kamhawi, H., Smith, T., Introduction, I., Thrusters, H., Bus, S., and Engineer, P., "High Throughput 600 Watt Hall Effect Thruster for Space Exploration," *52nd AIAA Joint Propulsion Conference*, AIAA-2016-4830, Salt Lake City, UT: 2016.

[9] Siddiqui, U., and Cretel, C., "Updated Performance Measurements and Analysis of the Phase Four RF Thruster," *2018 Joint Propulsion Conference*, AIAA-2018-4817, Cincinnati, OH: 2018, pp. 1–11.

[10] Cheng, S., and Martinez-Sanchez, M., "Hybrid Particle-in-Cell Erosion Modeling of Two Hall Thrusters," *Journal of Propulsion and Power*, 5, vol. 24, 2008, DOI: 10.2514/1.36179.

[11] Benavides, G. F., Kamhawi, H., Mackey, J., Haag, T., and Costa, G., "Iodine Hall-Effect Electric Propulsion System Research, Development, and System Durability Demonstration," *AIAA Joint Propulsion Conference*, AIAA-2018-4422, Cincinnati, OH: 2018.

[12] Frerking, M. A., and Beauchamp, P. M., "JPL Technology Readiness Assessment Guideline," *2016 IEEE Aerospace Conference*, Big Sky, MT: IEEE, 2016.

[13] Apollo Fusion Inc., "Apollo Xenon Engine (AXE)" Available: https://www.apollofusion.com/axe.html.

[14] Conversano, R. W., Goebel, D. M., Hofer, R. R., Matlock, T. S., and Wirz, R. E., "Development and Initial Testing of a Magnetically Shielded Miniature Hall Thruster," *IEEE Transactions on Plasma Science*, 1, vol. 43, 2015, DOI: 10.1109/TPS.2014.2321107.

[15] Conversano, R. W., Arora, N., Goebel, D. M., and Wirz, R. E., "Preliminary Mission Capabilities Assessment of a Magnetically Shielded Miniature Hall Thruster," *65th IAF/IAA/IISL International Astronaturical Congress*, IAC-14.C4.4.4, Toronto, Canada: 2014.

[16] Conversano, R. W., Goebel, D. M., Mikellides, I. G., Hofer, R. R., Matlock, T. S., and Wirz, R. E., "Magnetically Shielded Miniature Hall Thruster: Performance Assessment and Status Update," *50th AIAA Joint Propulsion Conference*, AIAA-2014-3896, Cleveland, OH: 2014.

[17] Conversano, R. W., Goebel, D. M., Hofer, R. R., Mikellides, I. G., Katz, I., and Wirz, R. E., "Magnetically Shielded Miniature Hall Thruster: Design Improvement and Performance Analysis," *34th ERPS International Electric Propulsion Conference*, IEPC-2015-100 / ISTS-2015-b-100, Kobe, Japan: 2015.

[18] Conversano, R. W., "Low-Power Magnetically Shielded Hall Thrusters," Ph.D. Thesis, Department of Mechanical and Aerospace Engineering, University of California, Los Angeles, 2015.

[19] Conversano, R. W., Arora, N., Strange, N. J., and Goebel, D. M., "An Enabling Low-Power Magnetically Shielded Hall Thruster for Interplanetary Smallsat Missions," *Interplanetary Small Satellite Conference*, Pasadena, CA: 2016.

[20] Conversano, R. W., Goebel, D. M., Hofer, R. R., and Arora, N., "Performance enhancement of a long-life, low-power hall thruster for deep-space smallsats," *IEEE Aerospace Conference*, Big Sky, MT: 2017.

[21] Conversano, R. W., Goebel, D. M., Hofer, R. R., Mikellides, I. G., and Wirz, R. E., "Performance analysis of a low-power magnetically shielded hall thruster: Experiments," *Journal of Propulsion and Power*, 4, vol. 33, 2017, DOI: 10.2514/1.B36230.

[22] Conversano, R. W., Goebel, D. M., Mikellides, I. G., Hofer, R. R., and Wirz, R. E., "Performance analysis of a low-power magnetically shielded hall thruster: Computational modeling," *Journal of Propulsion and Power*, 4, vol. 33, 2017, DOI: 10.2514/1.B36231.

[23] Conversano, R. W., Lobbia, R. B., Tilley, K. C., Goebel, D. M., Reilly, S., Mikellides, I. G., and Hofer, R. R., "Development and Initial Performance Testing of a Low-Power Magnetically Shielded Hall Thruster with an Internally-Mounted Hollow Cathode," *35th International Electric Propulsion Conference*, IEPC-2017-64, Atlanta, GA: 2017.

[24] Conversano, R. W., Lobbia, R. B., Kerber, T. V., Tilley, K. C., Goebel, D. M., Reilly, S. W., Mikellides, I. G., and Hofer, R. R., "Performance Characterization of a Low-Power Magnetically Shielded Hall Thruster with an Internally-Mounted Hollow Cathode," *Plasma Sources Science and Technology*, 2019.

[25] Lobbia, R., Conversano, R., Lopez Ortega, A., Reilly, S., and Mikellides, I., "Pole Erosion Measurements for the Development Model of the Magnetically Shielded Miniature Hall Thruster (MaSMi-DM)," *36th International Electric Propulsion Conference*, IEPC-2019-298, Vienna, Austria: 2019.

[26] Lopez Ortega, A., Mikellides, I. G., Conversano, R. W., Lobbia, R. B., and Chaplin, V. H., "Plasma Simulations for the Assessment of Pole Erosion in the Magnetically Shielded Miniature (MaSMi) Hall Thruster," *36th International Electric Propulsion Conference*, IEPC-2019-281, Vienna, Austria: 2019.

[27] Chaplin, V. H., Conversano, R. W., Lopez Ortega, A., Mikellides, I. G., Lobbia, R. B., and hofer, "Ion Velocity Measurements in the Magnetically Shielded Miniature Hall Thruster (MaSMi) Using Laser-Induced Fluorescence," *36th International Electric Propulsion Conference*, IEPC-2019-531, Vienna, Austria: 2019.

[28] Conversano, R. W., Barchowsky, A., Lobbia, R. B., Chaplin, V. H., Lopez Ortega, A., Loveland, J. A., Lui, A. D., Becatti, G., Reilly, S. W., Goebel, D. M., Snyder, J. S., Hofer, R. R., Randolph, T. M., Mikellides, I. G., Vorperian, V., Carr, G. A., Rapinchuk, J., Villalpando, C. Y., and Grebow, D., "Overview of the Ascendant Sub-kW Transcelestial Electric Propulsion System (ASTRAEUS)," *36th International Electric Propulsion Conference*, IEPC-2019-282, Vienna, Austria: 2019.

[29] Hofer, R. R., Kamhawi, H., Herman, D., Polk, J. E., Snyder, J. S., Mikellides, I., Huang, W., Myers, J., Yim, J., Williams, G., Lopez Ortega, A., Jorns, B., Sekerak, M., Griffiths, C., Shastry, R., Haag, T., Verhey, T., Gilliam, B., Katz, I., Goebel, D. M., Anderson, J. R., Gilland, J., and Clayman, L., "Development Approach and Status of the 12.5 kW HERMeS Hall Thruster for the Solar Electric Propulsion Technology Demonstration Mission," *34th International Electric Propulsion Conference*, IEPC-2015-186, Kobe, Japan: 2015.

[30] Hofer, R., Polk, J., Sekerak, M., Mikellides, I., Kamhawi, H., Verhey, T., Herman, D., and Williams, G., "Development Status of the 12.5 kW HERMeS Hall Thruster for the Solar Electric Propulsion Technology Demosntration Mission," *52nd AIAA Joint Propulsion Conference*, AIAA-2016-4825, Salt Lake City, UT: 2016.

[31] Hofer, R., Polk, J. E., Mikellides, I. G., Lopez Ortega, A., Conversano, R. W., Chaplin, V. H., Lobbia, R. B., Goebel, D. M., Kamhawi, H., Verhey, T., Williams, G., Mackey, J., Huang, W., Yim, J., Herman, D. A., and Peterson, P. Y., "Development Status of the 12.5 kW Hall Effect Rocket with Magnetic Shielding (HERMeS)," *35th International Electric Propulsion Conference*, IEPC-2017-231, Atlanta, GA: 2017.

[32] Grys, K. De, Mathers, A., and Welander, B., "Demonstration of 10,400 Hours of Operation on a 4.5 kW Qualification Model Hall Thruster," *46th AIAA Joint Propulsion Conference*, AIAA-2010-6698, Nashville, TN: 2010.

[33] Mikellides, I. G., Katz, I., Hofer, R. R., Goebel, D. M., de Grys, K., and Mathers, A., "Magnetic shielding of the channel walls in a Hall plasma accelerator," *Physics of Plasmas*, 033501, vol. 18, 2011, DOI:

10.1063/1.3551583.
[34] Mikellides, I. G., Katz, I., Hofer, R. R., and Goebel, D. M., "Design of a Laboratory Hall Thruster with Magnetically Shielded Channel Walls, Phase III: Comparison of Theory with Experiment," *48th AIAA Joint Propulsion Conference*, AIAA-2012-3789, Atlanta, GA: 2012.
[35] Hofer, R. R., Goebel, D. M., Mikellides, I. G., and Katz, I., "Design of a Laboratory Hall Thruster with Magnetically Shielded Channel Walls, Phase II: Experiments," *48th AIAA Joint Propulsion Conference*, AIAA-2012-3788, Atlanta, GA: 2012.
[36] Mikellides, I. G., Katz, I., Hofer, R. R., and Goebel, D. M., "Magnetic shielding of walls from the unmagnetized ion beam in a Hall thruster," *Applied Physics Letters*, 023509, vol. 102, 2013, DOI: 10.1063/1.4776192.
[37] Mikellides, I. G., Katz, I., Hofer, R. R., and Goebel, D. M., "Magnetic shielding of a laboratory Hall thruster. I. Theory and validation," *Journal of Applied Physics*, 043303, vol. 115, 2014, DOI: 10.1063/1.4862313.
[38] Hofer, R. R., Goebel, D. M., Mikellides, I. G., and Katz, I., "Magnetic shielding of a laboratory Hall thruster. II. Experiments," *Journal of Applied Physics*, 043303, vol. 115, 2014, DOI: 10.1063/1.4862313.
[39] Mikellides, I. G., Katz, I., Hofer, R. R., Goebel, D. M., de Grys, K., and Mathers, A., "Magnetic shielding of the channel walls in a Hall plasma accelerator," *Physics of Plasmas*, 033501, vol. 18, 2011, DOI: 10.1063/1.3551583.
[40] Hofer, R. R., Jorns, B. A., Polk, J. E., Mikellides, I. G., and Snyder, J. S., "Wear test of a magnetically shielded Hall thruster at 3000 seconds specific impulse," *33rd International Electric Propulsion Conference*, IEPC-2013-033, Washington D.C.: 2013.
[41] Mikellides, I. G., Hofer, R. R., Katz, I., and Goebel, D. M., "Magnetic shielding of Hall thrusters at high discharge voltages," *Journal of Applied Physics*, 053302, vol. 116, 2014, DOI: 10.1063/1.4892160.
[42] Huang, W., Shastry, R., Soulas, G. C., and Kamhawi, H., "Farfield Plume Measurement and Analysis on the NASA-300M and NASA-300MS," *33rd International Electric Propulsion Conference*, IEPC-2013-057, Washington D.C.: 2013.
[43] Kamhawi, H., Huang, W., Haag, T. W., Shastry, R., Soulas, G. C., Smith, T., Mikellides, I. G., and Hofer, R. R., "Performance and Thermal Characterization of the NASA-300MS 20 kW Hall Effect Thruster," *33rd International Electric Propulsion Conference*, IEPC-2013-444, Washington D.C.: 2013.
[44] Conversano, R. W., Lobbia, R. B., Tilley, K. C., Goebel, D. M., Reilly, S. W., Mikellides, I. G., and Hofer, R. R., "Development and Initial Performance Testing of a Low-Power Magnetically Shielded Hall Thruster with an Internally-Mounted Hollow Cathode," *35th International Electric Propulsion Conference*, IEPC-2017-64, Atlanta, GA: 2017.
[45] Conversano, R. W., Goebel, D. M., Katz, I., and Hofer, R. R., "Low-Power Hall Thrsuter with an Internally Mounted Low-Current Hollow Cathode," US Patent No. 16/205,048, 2019.
[46] Conversano, R. W., Goebel, D. M., Hofer, R. R., Matlock, T. S., and Wirz, R. E., "Magnetically Shielded Miniature Hall Thruster : Development and Initial Testing," *33rd ERPS International Electric Propulsion Conference*, IEPC-2013-201, Washington D.C.: 2013.
[47] Katz, I., Mikellides, I. G., Jorns, B. A., and Lopez Ortega, A., "Hall2De Simulations with an Anomalous Transport Model Based on the Electron Cyclotron Drift Instability," *34th International Electric Propulsion Conference*, IEPC-2015-402 / ISTS-2015-b-402, Kobe, Japan: 2015.
[48] Lopez Ortega, A., Mikellides, I. G., and Katz, I., "Hall2De Numerical Simulations for the Assessment of Pole Erosion in a Magnetically Shielded Hall Thruster," *34th International Electric Propulsion Conference*, IEPC-2015-249 / ISTS-2015-b-249, Kobe, Japan: 2015.
[49] Mikellides, I. G., "Hall2De Simulations with a First-Principles Electron Transport Model Based on the Electron Cyclotron Drift Instability," *52nd AIAA Joint Propulsion Conference*, AIAA-2016-4618, Salt Lake City, UT: 2016.
[50] Sekerak, M. J., Hofer, R. R., Polk, J. E., Jorns, B. A., and Mikellides, I. G., "Wear Testing of a Magnetically Shielded Hall Thruster at 2000 s Specific Impulse," *34th International Electric Propulsion Conference*, IEPC-2015-155, Kobe, Japan: 2015.
[51] Goebel, D. M., Jorns, B. A., Hofer, R. R., Mikellides, I. G., and Katz, I., "Pole-piece Interactions with the Plasma in a Magnetically Shielded Hall Thruster," *50th AIAA Joint Propulsion Conference*, AIAA 2014-3899, Cleveland, OH: 2014.
[52] Jorns, B. A., "Mechanisms for Pole Piece Erosion in a 6-kW Magnetically-Shielded Hall Thruster," *52nd AIAA/ASME/SAE/ASEE Joint Propulsion Conference*, AIAA-2016-4839, Salt Lake City, UT: 2016.
[53] Hofer, R. R., Cusson, S., and Lobbia, R. B., "The H9 Magnetically Shielded Hall Thruster," *35th International Electric Propulsion Conference*, IEPC-2017-232, Atlanta, GA: 2017.

[54] Hofer, R. R., Johnson, L. K., Goebel, D. M., and Fitzgerald, D. J., "Effects of an Internally-Mounted Cathode on Hall Thruster Plume Properties," *IEEE Transactions on Plasma Science*, 5, vol. 36, 2006, DOI: 10.1109/TPS.2008.2000962.
[55] Mcdonald, M. S., Gallimore, A. D., and Arbor, A., "Cathode Position and Orientation Effects on Cathode Coupling in a 6-kW Hall Thruster," *31st International Electric Propulsion Conference*, IEPC-2009-113, Ann Arbor, MI: 2009.
[56] Loyan, A., Titov, M., Rybalov, O., and Maksymenko, T., "Middle power Hall Effect Thrusters with centrally located cathode," *33rd International Electric Propulsion Conference*, IEPC-2013-410, Washington D.C.: 2013.
[57] Hofer, R. R., Goebel, D. M., and Watkins, R. M., "Compact LaB 6 Hollow Cathode for the H6 Hall Thruster," *54th JANNAF Propulsion Meeting*, Denver, CO: 2007.
[58] Hofer, R. R., and Anderson, J. R., "Finite Pressure Effects in Magnetically Shielded Hall Thrusters," *50th AIAA Joint Propulsion Conference*, AIAA-2014-3709, Cleveland, OH: 2014.
[59] Frieman, J. D., Kamhawi, H., Williams, G., Herman, D. A., Peterson, P. Y., Gilland, J. H., and Hofer, R. R., "Long Duration Wear Test of the NASA HERMeS Hall," *2018 Joint Propulsion Conference*, AIAA-2018-4645, Cincinnati, OH: 2018.
[60] Ho, A., Jorns, B. A., Mikellides, I. G., Goebel, D. M., and Lopez Ortega, A., "Wear Test Demonstration of a Technique to Mitigate Keeper Erosion in a High-Current LaB6 Hollow Cathode," *52nd AIAA/SAE/ASEE Joint Propulsion Conference*, AIAA-2016-4836, Salt Lake City, UT: 2016.
[61] Benavides, G. F., Kamhawi, H., Liu, T. M., Pinero, L. R., Verhey, T. R., Rhodes, R., Yim, J. T., Mackey, J. A., Gray, T. G., Butler-Craig, N. I., Myers, J. L., and Birchenough, A. G., "Development of a High-Propellant Throughput Small Spacecraft Electric Propulsion System to Enable Lower Cost NASA Science Missions," *AIAA Propulsion and Energy Forum*, AIAA-2019-4162, Indianapolis, IN: 2019.
[62] Huang, W., Yim, J., and Kamhawi, H., "Design and Empirical Assessment of the HERMeS Hall Thruster Propellant Manifold," *62nd JANNAF Propulsion Meeting*, Nashville, TN: 2015.
[63] Reilly, S., Sekerak, M. J., and Hofer, R. R., "Transient Thermal Analysis of the 12.5 kW HERMeS Hall Thruster," *52nd AIAA/SAE/ASEE Joint Propulsion Conference*, AIAA-2016-5024, Salt Lake City, UT: 2016.
[64] Myers, J., Kamhawi, H., Yim, J. T., and Clayman, L., "Hall Thruster Thermal Modeling and Test Data Correlation," *52nd AIAA/SAE/ASEE Joint Propulsion Conference*, AIAA-2016-4535, Salt Lake City, UT: 2016.
[65] Goebel, D., and Katz, I., *Fundamentals of Electric Propulsion: Ion and Hall Thrusters*, Hoboken, NJ: John Wiley & Sons, Inc., 2008.
[66] Incropera, F. P., and DeWitt, D. P., *Introduction to Heat Transfer*, University of California: Wiley, 1985.
[67] Mikellides, I. G., and Katz, I., "Numerical simulations of Hall-effect plasma accelerators on a magnetic-field-aligned mesh," *Physical Review E - Statistical, Nonlinear, and Soft Matter Physics*, 4, vol. 86, 2012, DOI: 10.1103/PhysRevE.86.046703.
[68] Donabedian, M., *Spacecraft Thermal Control Handbook, Volume II: Cryogenics*, American Institute of Aeronautics and Astronautics, 2003.
[69] Reilly, S. W., Lobbia, R. B., Conversano, R. W., and Hofer, R. R., "Thermal Analysis and Testing of the 12.5 kW HERMeS Hall Thruster," *30th NASA Thermal Fluids Analysis Workshop*, TFAWS19-ID-18, Hampton, VA: 2019.